Structural Changes in Poly(2-methoxyethyl acrylate) Thin Films Induced by Absorption of Bisphenol A. An Infrared and Sum Frequency Generation (SFG) Study

Shen Ye,*,†,‡,§ Shigeaki Morita,‡ Guifeng Li,§ Hiroyuki Noda,‡ Masaru Tanaka,|| Kohei Uosaki,⊥ and Masatoshi Osawa†,§

Catalysis Research Center, Hokkaido University, Sapporo 060-0811, Japan; PRESTO, Japan Science and Technology Corporation (JST), Tokyo, Japan; Graduate School of Environmental Earth Science, Hokkaido University, Sapporo 060-0810, Japan; Research Institute for Electronic Science, Hokkaido University, Sapporo 060-0812, Japan; and Division of Chemistry, Graduate School of Science, Hokkaido University, Sapporo 060-0810, Japan

Received December 27, 2002; Revised Manuscript Received May 6, 2003

ABSTRACT: The structural changes in poly(2-methoxyethyl acrylate) (PMEA) thin films induced by the absorption of bisphenol A (BPA), which is suspected to be an endocrine disrupter disturbing the hormone balance in a living body, have been investigated by infrared reflection absorption spectroscopy (IRRAS) and sum frequency generation (SFG) measurements. BPA molecules are absorbed in PMEA thin film. By controlling the thickness of the intermediate polystyrene (PS) film between the PMEA and Au substrate, we are able to probe the molecular structure at the different PMEA interfaces of air/PMEA (free) and PMEA/PS (buried) by the SFG measurements. The ether methyl (OCH_3) group in the side chain of PMEA at both interfaces has the same vector orientation with respect to Au, i.e., pointing into air at the free interface and pointing into PMEA at the PMEA/PS buried interface. The OCH_3 groups at the PMEA interfaces are likely to stand up and that the interfacial ordering on the PMEA is increased by the BPA absorption. The structural changes in the PMEA bulk and its interface induced by BPA absorption and desorption are reversible.

Introduction

Bisphenol A (BPA, Chart 1a) is widely used as a monomer for the synthesis of polycarbonate (PC). It has been reported that BPA can be dissolved from PC products such as food packaging and is suspected to disturb the hormone balance in a living body; i.e., it is considered an endocrine disrupter (i.e., an environmental hormone).[1,2] However, details about the interaction and penetration mechanisms of BPA with living organisms are still not well-known at the molecular level.

Recently, Tanaka et al. synthesized a new biocompatible polymer, poly(2-methoxyethyl acrylate) (PMEA, Chart 1b) and reported that it has an excellent blood compatibility featuring a significantly low adsorption of plasma protein and low platelet adhesion in comparison with other poly(acrylate)s.[3] PMEA is expected to be a promising biomaterial and is now commercially used as a coating material for artificial organs.[4] Due to its superior biocompatibility, the PMEA thin film is used as a model of biological membranes to elucidate the interaction between BPA and the living body in the present study.

The structural changes in the PMEA thin film induced by the absorption and desorption of BPA have been investigated by infrared reflection absorption spectroscopy (IRRAS) and sum frequency generation (SFG) measurements in this study. IRRAS measurement[5] can provide valuable information about the structural changes in the PMEA bulk while SFG measurement[6−9] is employed to clarify the molecular structures on the PMEA interfaces. These results were compared with the behavior observed on poly(methyl methacrylate) (PMMA, Chart 1c) and polystyrene (PS, Chart 1d) thin films. BPA molecules were absorbed in PMEA bulk but were not absorbed in PMMA and PS thin films. The absorbed BPA can be removed from the PMEA by an ethanol rinsing treatment. By controlling the thickness of a polystyrene (PS) layer sandwiched

Chart 1. Molecular Structures of (a) Bisphenol A (BPA), (b) Poly(2-methoxyethyl acrylate) (PMEA), (c) Poly(methyl methacrylate) (PMMA), (d) Polystyrene (PS), and (e) Deuterated Polystyrene (dPS)

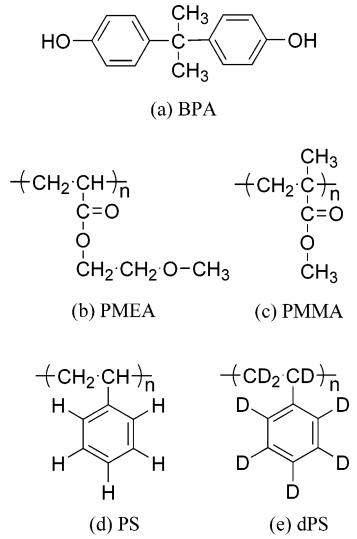

* To whom correspondence should be addressed. E-mail: ye@cat.hokudai.ac.jp.
† Catalysis Research Center, Hokkaido University.
‡ PRESTO, Japan Science and Technology Corporation (JST).
§ Graduate School of Environmental Earth Science, Hokkaido University.
|| Research Institute for Electronic Science, Hokkaido University.
⊥ Division of Chemistry, Graduate School of Science, Hokkaido University.

10.1021/ma026007d CCC: $25.00
Published on Web 06/20/2003

between PMEA and Au substrate, we are able to selectively measure the molecular structures at air/PMEA (free) and PMEA/PS (buried) interfaces by the SFG measurements. The experimental results demonstrate that the OCH_3 groups on the PMEA interfaces are likely to stand up and that the ordering of the PMEA interfaces also becomes higher after the BPA molecules were absorbed. These structural changes in the PMEA bulk and interfaces induced by the absorption and desorption of BPA are reversible. Reasons for the selective absorption of BPA in PMEA thin films are discussed based on these results.

Experimental Section

Sample Preparation. PMEA ($M_w \sim 8.5 \times 10^4$) was prepared by the radical polymerization method as reported previously[3]. PMMA ($M_w \sim 12.0 \times 10^4$, Aldrich), which has a structure similar to that of PMEA, PS ($M_w \sim 4.5 \times 10^4$, Aldrich), and deuterated polystyrene (dPS, $M_w \sim 14.3 \times 10^4$, Polymer Source, Chart 1e) were used for comparison. BPA and organic solvents were purchased from Wako Pure Chemical Industries. All chemicals were used without further purification. Milli-Q water was used to prepare aqueous solutions.

A 200 nm-thick Au film evaporated on a glass plate (25 mm × 25 mm × 1 mm) was used as the substrate. PMEA thin films were deposited from a 10 g·L^{-1} methanol solution by spin coating: a 200 μL solution was dropped on the substrate, and the sample was then rotated at 500 rpm for 2 s and then at 1000 rpm for 20 s, and then dried for 30 min in the chamber of the spin coater saturated with the solvent vapor. Because dewetting of PMEA on the Au substrate was observed in water, a PS or a dPS thin layer was sandwiched between PMEA and the Au substrate to increase its stability. In the present paper, we fixed the thickness of PMEA films and changed the thickness of the PS thin films between PMEA and the Au substrate. The thickness of the PS films was controlled by the PS concentration in its toluene solutions (1−25 g·L^{-1}).

SFG Measurements. A detailed description of the broad-band SFG system used in the present study has been given elsewhere.[10] Briefly, a Ti:sapphire laser (Hurricane, Spectra Physics) was employed as a light source. A tunable broad-band infrared pulse (~200 cm^{-1} fwhm) from 3700 to 1000 cm^{-1} was generated from an optical parametric amplifier system (TOPAS, light conversion). A narrow-band visible pulse (<10 cm^{-1} fwhm) at 800 nm was yielded from the spectral shaper (TII). The infrared and visible pulses were temporally and spatially overlapped at the sample surface at incident angles with respect to the surface normal of 50° and 65°, respectively. The reflected SFG signal was dispersed with a monochromator (MS3501i, Solar-TII) and was detected by a CCD (DU420−BV, Andor Technology) cooled to −70 °C. All spectra were accumulated for 10 min in the ssp polarization (i.e., s-polarized SFG, s-visible, and p-infrared).

The SFG signal from the polymer samples was normalized with the SFG signal from GaAs. Assuming that the SFG signals resonate only with infrared light (ω_{IR}), the SFG spectra were fitted by a Lorentzian function:[6,11]

$$I_{SFG}(\omega_{IR}) = \left| \sum_n \frac{A_n}{\omega_{IR} - \omega_n + i\Gamma_n} + \left|\chi_{NR}^{(2)}\right| \exp(-i\phi) \right|^2 \quad (1)$$

where A_n, ω_n and Γ_n are the amplitude, peak position and bandwidth of the nth resonant mode, respectively, and $|\chi_{NR}^{(2)}|$ and ϕ are the amplitude of the nonresonant (NR) contribution and its relative phase angle, respectively.

IRRAS Measurements. A Bio-Rad FTS 575C FT-IR spectrometer equipped with a liquid-N_2 cooled HgCdTe detector and a Harrick Reflector grazing angle reflectance unit (incident angle: 75°) was used for the IRRAS measurements. All IRRAS spectra were obtained by coadding 32 interferrograms with a spectral resolution of 4 cm^{-1}.

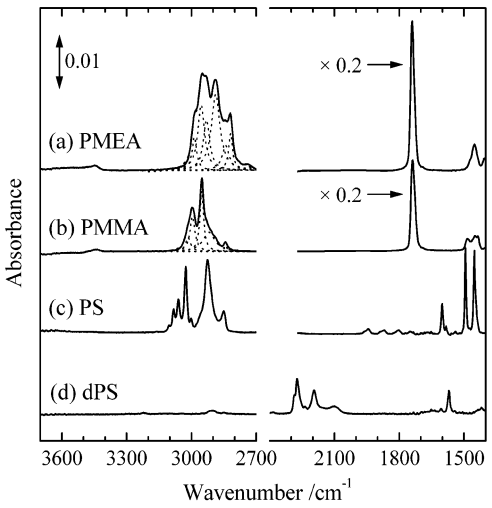

Figure 1. IRRAS spectra of (a) PMEA, (b) PMMA, (c) PS, and (d) dPS thin films on the Au.

AFM Measurements. The morphologies of each polymer surface were characterized by an atomic force microscope (AFM) with a NPX 100 scanner head and a Nanopics 1000 controller (Seiko Instruments) under a damping mode. The root-mean-square (RMS) roughness for PMEA surface was ca. 1.6 nm, indicating that the PMEA surface is relatively smooth. Similar results have also been obtained on the other polymer surfaces.

Ellipsometry Measurements. The thickness of the polymer sample was determined by an ellipsometry measurement[12] with a SOPRA GESP-5 spectrometer using a 30 W Xe lamp as a light source.[13] The incident angle was 75°. As shown in eq 2, Ψ and Δ correspond to the modulus and phase for the ratio of polarized reflection coefficients (R_p and R_s), respectively, and were measured at 300−800 nm at steps of 10 nm.

$$\frac{R_p}{R_s} = (\tan \Psi) \exp(i\Delta) \quad (2)$$

The thicknesses of PMEA and PS thin films were calculated by simulations using WinElli software (SOPRA).[13] The complex dielectric function for the Au substrate was determined using a bare Au substrate. The imaginary parts of the complex dielectric function for the PMEA and PS were assumed to be zero because they have negligible absorption in 300−800 nm. After the thickness of the PS or dPS film on the Au surface was determined using a three-layer model (air/PS/Au) by iterative fitting procedures, PMEA was deposited and its thickness was determined using a four-layer model (air/PMEA/PS/Au) by the same procedures. The thickness of the PMEA thin film deposited on the PS/Au substrate from a 10 g·L^{-1} methanol solution was determined to be 75.0 ± 1.0 nm, which was employed for all samples in the present study.

Results and Discussion

1. Absorption of BPA in the Bulk of the Polymer Thin Film. 1.1. IRRAS Characterization of the Polymer Thin Films. Figure 1 shows the IRRAS spectra of thin films of (a) PMEA, (b) PMMA, (c) PS, and (d) dPS deposited on Au substrates in the region of 3700−2700 cm^{-1} and 2400−1400 cm^{-1}. In addition to the intense peak at 1740 cm^{-1} corresponding to the C=O stretching of the carbonyl group, PMEA and PMMA thin films have broad IR absorption with several peaks and shoulders in the C−H stretching region (Figure 1a,b).[14−16] The C−H stretching region (3400−2700 cm^{-1}) of the two spectra were deconvoluted, and the results are shown as dotted lines in the same figures. The peak positions and their assignments are summarized in

Table 1. Assignments of IRRAS Spectra of Polymers

polymer	wavenumber/cm^{-1}	assignment[a]
PMEA	2986	OCH_3 ν_{as}
	2955	OCH_2 ν_{as}
	2930	CCH_2 ν_{as}
	2888	OCH_2 ν_s
	2841	CCH_2 ν_s
	2819	OCH_3 ν_s
	1740	C=O stretching
	1500−1400	C−H deformation bands
PMMA	3015	OCH_3 ν_{as}
	2995	OCH_3 ν_{as}, α-CH_3 ν_{as}
	2952	OCH_3 ν_s, α-CH_3 ν_{as}
	~2920	α-CH_3 ν_s, CH_2 ν_{as}
	2841	CH_2 ν_s
	1740	C=O stretching
	1500−1400	C−H deformation bands
PS	3083	ring ν_{20a}
	3060	ring ν_2
	3026	ring ν_{20b}
	2924	CH_2 ν_{as}
	2851	CH_2 ν_s
	2000−1700	summation bands
	1600−1400	ring C−C stretching bands
dPS	2288	ring ν_2
	2272	ring ν_{20b}
	2194	CD_2 ν_{as}
	2109	CD_2 ν_s
	1600−1400	ring C−C stretching bands

[a] ν_s: symmetric stretching. ν_{as}: asymmetric stretching.

Table 1. The peaks for asymmetric and symmetric C−H stretching of the terminal OCH_3 group in the side chain of the PMEA thin film were observed at 2986 and 2819 cm^{-1}, respectively. On the other hand, the corresponding modes for PMMA were located at 3015, 2995, and 2952 cm^{-1}, respectively. The difference in the peak position of the OCH_3 modes should be attributed to the different chemical environment for the terminal OCH_3 group in PMEA (ether type) and PMMA (ester type).

In addition to the two C−H stretching vibrations from the polymer main chain at 2851 and 2924 cm^{-1}, the PS thin film shows a number of peaks above 3000 cm^{-1} (Figure 1c), which can be assigned to the C−H stretching modes of the phenyl ring (Table 1). The C−C ring stretching modes observed at 1600−1400 cm^{-1} show typical features of the monosubstituted benzenes.[14] The detailed assignments for the main peaks in the IRRAS spectrum of PS are given in Table 1 based on Wilson's notation.[17] In the case of the dPS film (Figure 1d), C−D stretching modes were shifted to the 2400−2100 cm^{-1} region due to the isotope effect (Table 1).

1.2. Structural Changes Induced by BPA Absorption in the Polymer Bulk. Figure 2a shows the IRRAS spectrum of a 75 nm thick PMEA film deposited on a Au substrate covered by a 90 nm dPS thin film (denoted as PMEA/dPS90nm/Au, same as below). By using dPS instead of PS, the IR contributions from PMEA (Figure 1a) and dPS (Figure 1d) can be separated completely in the C−H stretching region. After dipping this sample into a saturated (340 ppm) BPA aqueous solution for 10 s, remarkable changes were observed in the IRRAS spectrum (Figure 2b): A very broad peak around 3400 and three sharp peaks at 1616, 1603, and 1514 cm^{-1} were newly observed. These peaks are identical to those observed in the IR absorption spectrum of BPA in a KBr matrix (Figure 2d, Table 2), suggesting that BPA molecules were absorbed in the PMEA thin film after the immersion process. On the other hand, no spectral changes were observed for PMMA and PS (or dPS) after their immersion into the same BPA solution (IRRAS results are not shown here). These results demonstrated that BPA molecules absorb in PMEA but not in PMMA and PS thin films and are in agreement with our recent BPA absorption results obtained by in situ quartz crystal microbalance (QCM) measurements.[18]

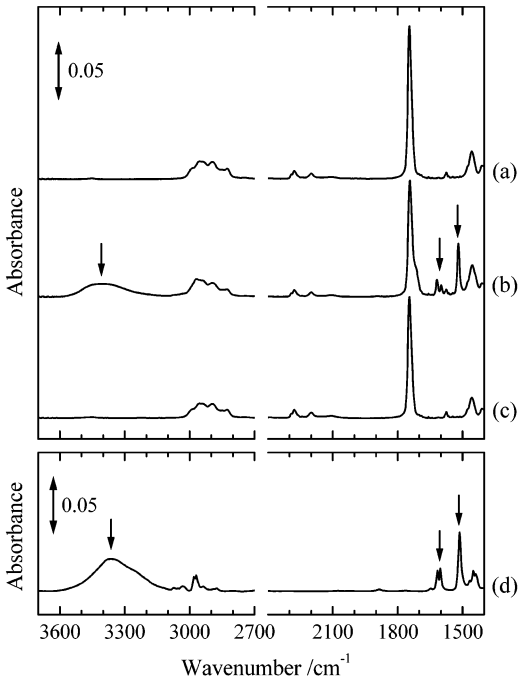

Figure 2. Top: IRRAS spectra of PMEA/dPS90nm/Au. (a) original sample, (b) sample after 10 s dipping in a saturated BPA solution, and (c) sample after rinsing sample b with ethanol. Bottom: (d) IR absorption spectrum of BPA in a KBr matrix.

Table 2. Assignment of IR Spectrum of BPA

wavenumber/cm^{-1}	assignment
~3400	O−H stretching
3072	ring ν_2
2969	CH_3 ν_{as}
2873	CH_3 ν_s
1616	ring ν_{8a}
1603	ring ν_{8b}
1514	ring ν_{19a}
1450	ring ν_{19b}

It is also interesting to note that a shoulder appeared around 1726 cm^{-1} on the C=O stretching band of carbonyl group at 1740 cm^{-1} of PMEA after immersion in BPA-saturated aqueous solution (Figure 1b). This shoulder indicates that hydrogen bonding is formed between the carbonyl group in PMEA and the hydroxyl group in BPA.[14] Similar phenomena were also observed in the polymer blend of poly(4-vinylphenol) and PMMA.[19]

However, after rinsing of the immersed sample in ethanol for a few seconds, the peaks due to BPA absorption disappeared completely (Figure 2c), and the IRRAS spectrum became almost identical to that obtained without immersion in BPA solution (Figure 1a). It is evident that the absorbed BPA can be readily removed by the ethanol solvent while the polymer structure remains virtually unchanged. Hence, the absorption and desorption of BPA in PMEA thin films is reversible. However, the absorbed BPA cannot be removed by water rinsing only.

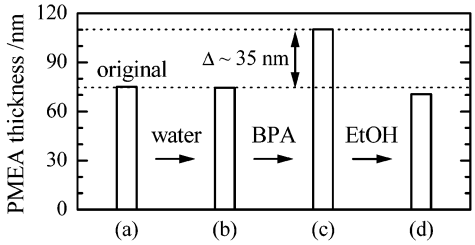

Figure 3. Thickness of the PMEA layer of PMEA/dPS7nm/Au measured by ellipsometry: (a) original sample, (b) sample after 10-s dipping in water, (c) sample after 10 s dipping in saturated BPA solution, and (d) sample after rinsing with ethanol.

The amount of BPA molecules absorbed into the PMEA thin film was estimated from the intensity of the characteristic peak of BPA at 1514 cm^{-1} in comparison with the IRRAS spectrum of a mixed film of PMEA + BPA (1:1 in weight, from 10 $g \cdot L^{-1}$ methanol solution). It is roughly estimated that ca. 35 wt % BPA relative to PMEA penetrated into the PMEA thin film on dipping in the saturated BPA aqueous solution for 10 s (Figure 2b). That is, BPA is significantly condensed in the PMEA thin film (more than 1000 times) compared with that in the saturated solution (340 ppm). Of course, the condensation degree also depends on the film thickness of PMEA and the concentration of BPA as well as immersion time.[18]

1.3. Changes in Thickness of the PMEA Thin Films by the Absorption and Desorption of BPA. As shown above, a large amount of BPA molecules absorbed reversibly in the PMEA thin films. To understand the interaction between BPA and the PMEA bulk in detail, its thickness changes during the BPA absorption and desorption processes were characterized by ex situ ellipsometry measurements. As shown in Figure 3, although no change in the film thickness was observed after immersing the PMEA/dPS7nm/Au sample into pure water, the thickness of the PMEA increased to 110 nm ($\Delta \sim$35 nm) after dipping in the BPA-saturated solution for 10 s. Furthermore, after desorption of BPA by an ethanol rinsing treatment, the PMEA thickness decreased to 71.0 nm, slightly thinner than that of the PMEA (75 nm) before BPA absorption. Small morphological changes on the PMEA thin film could be observed after the complete evaporation of the ethanol solvent from the polymer surface.

Similar increases in thickness were also observed on the PMEA thin films with different thicknesses of the PS films on the Au substrates, indicating that the PMEA film swells due to the BPA absorption. This swelling process is a relatively reversible one after BPA removal by ethanol. A better reversibility of the PMEA morphology should be obtained if the solvent is optimized.

2. Structural Changes in Polymer Thin Film Interfaces Induced by BPA Absorption. As described above, BPA molecules absorb selectively in PMEA but do not absorb in PMMA or PS thin films. The molecular structure on the polymer interface should play a role in the BPA absorption in the polymer thin films and is especially useful for recognizing the nature of the interaction between BPA and the biological membranes. However, such an interface-specific structural change is hardly obtained by IRRAS measurement.

As a second-order nonlinear vibration spectroscopy, SFG[6,7] is a powerful means for exploring interfacial structures at different interfaces (vapor/liquid,[20] liquid/solid,[11,21,22] liquid/liquid,[8,22] polymer,[9,23,24] etc.) with high selectivity and sensitivity. In the following section, we will first show that the molecular structures at the different polymer interfaces (air/PMEA or PMEA/PS) can be probed selectively by controlling the thickness of the sandwiched PS film between PMEA and the Au substrate. We will then show the structural changes at the interfaces of the PMEA thin film induced by BPA absorption in comparison with the IRRAS results for BPA absorption in the PMEA bulk. The adsorption of BPA on the free surfaces of PMMA and PS thin films into which BPA molecules cannot penetrate will also be discussed.

2.1. Thickness-Dependent SFG Spectra for PMEA/PS/Au System. SFG signals from a centrosymmetric polymer bulk are forbidden in the electric dipole approximation and can arise only from the polymer interfaces.[6] Therefore, a number of interfaces, such as air/polymer, polymer/polymer, and polymer/substrate, may be observed by SFG measurement in the present PMEA/PS/Au system. We need to determine which interfaces mainly contribute to the SFG spectra in the first step. The contribution of the SFG signals is controlled by the relative intensity of the local electric field at each interface. Dhinojwala et al. demonstrated that the molecular structure on the PS/air and PS/sapphire substrate could be explored separately by choosing the incident angle of the input beams with a total internal reflection geometry.[25] Chen et al. showed that the buried interface between PS and poly(*n*-butyl methacrylate) (PBMA) thin films can be detected by shining IR and visible light from the backside of the fused silica substrate.[26]

On the other hand, when the thickness of the intermediate optical layer is comparable to the SFG wavelength, the interference effect between the reflected and transmitted SFG lights can be employed to enhance SFG signals from the desired interface while minimizing those from other interfaces. Recently, Richter et al. investigated the interfacial structures of the 129 nm thick PS thin film on SiO_2 film (140−330 nm) deposited on a Au substrate and reported that the SFG spectra of PS depended on the thickness of the SiO_2 film between the PS and the Au substrate.[27,28] The thickness dependence of the SFG signals was analyzed quantitatively by considering the constructive optical interference of reflected and transmitted SFG light and the optimization for probing free and buried PS interfaces was realized by controlling the thickness of the intermediate SiO_2 film. As will be shown below, we have also independently observed the PS thickness-dependent SFG spectra in the case of PMEA/PS/Au system, and we are able to detect the polymer/polymer or polymer/air interface by changing the thickness of the PS films.

Figure 4 shows the SFG spectra of a 75 nm thick PMEA film deposited on the Au substrate covered by various thicknesses of PS films (0−220 nm) in the C−H stretching region (2750−3100 cm^{-1}). The SFG curves were offset vertically for clarity with the zero points for each curve indicated in the same figure. It is interesting to note that both the resonance and the NR SFG signals significantly depend on the thickness of the PS film sandwiched between PMEA and the Au substrate.

When the thickness of PS is less than 10 nm (Figure 4a,b), a number of downward peaks can be observed at 2800−3000 cm^{-1}. These downward peaks can be mainly

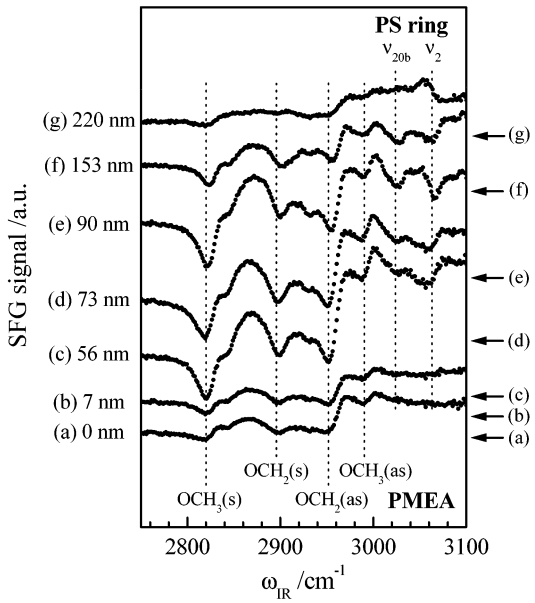

Figure 4. SFG spectra of PMEA/PS/Au with different thicknesses of the PS layer of (a) 0, (b) 7, (c) 56, (d) 73, (e) 90, (f) 153, and (g) 220 nm. Zero level of each spectra is shown by arrows on the right side.

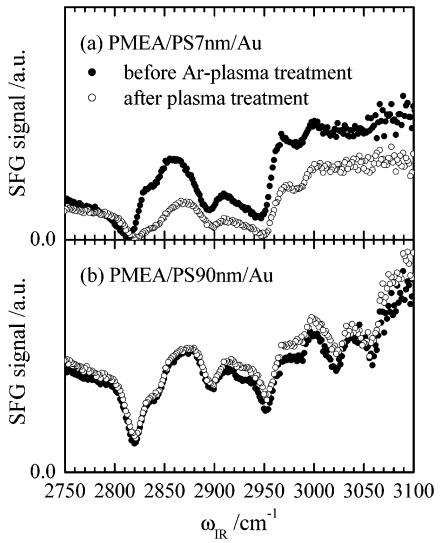

Figure 5. SFG spectra of (a) PMEA/PS7nm/Au and (b) PMEA/PS90nm/Au. Black and white circles correspond to before and after 5 s Ar-plasma treatment, respectively.

assigned to symmetric and asymmetric C−H stretching of the OCH_3 and OCH_2 moieties in the side chain of the PMEA as indicated by the dotted lines in Figure 4. Two downward peaks around 2822 and 2990 cm^{-1} are important features for C−H stretching modes of the OCH_3 group in PMEA (Table 1). No apparent peak was observed in a frequency region higher than 3000 cm^{-1} (Figure 4a,b) where the C−H stretching modes of the phenyl ring in the PS film are located (Figure 1c, Table 1). Because no peaks for PS, but only those for PMEA, were observed in the SFG spectra of PMEA/Au (Figure 4a) and PMEA/PS7nm/Au (Figure 4b), these SFG spectra should be dominated only by the interfacial molecular structures at the air/PMEA interface.

When the thickness of the PS increased more (56−90 nm, Figure 4c−e), the intensities of the SFG peaks due to PMEA in the region between 2800 and 3000 cm^{-1} became larger than those with thinner PS layers (Figure 4a,b). At the same time, two downward peaks with similar intensity were newly observed around 3020 and 3060 cm^{-1}, which can be attributed to the ν_{20b} and ν_2 modes of PS, respectively. The intensities of the SFG peaks due to PMEA decreased while those for PS were almost the same at a PS thickness of 153 nm (Figure 4f). Furthermore, significant differences appeared at a PS thickness of 220 nm in Figure 4g. The intensities of the SFG peaks due to the PMEA between 2800 and 3000 cm^{-1} became even weaker, while the two peaks attributed to the ν_2 and ν_{20b} modes of PS were observed with a peak direction (upward) opposite to those with a thinner PS thickness (Figure 4c−f).

As shown in Figure 4c−f, both SFG peaks from PMEA and PS were observed in the PS thickness range between 56 and 153 nm. Either PMEA/PS or air/PMEA or even PS/Au interfaces may contribute to the SFG spectra (Figure 4c−f). Although a complete explanation for the above PS-thickness-dependent SFG requires detailed SFG measurements over a wider PS-thickness region as well as the calculations for the Fresnel coefficients as a function of the film thickness which will be given elsewhere,[29] these features shown in Figure 4 can be interpreted quantitatively by constructive interference between the reflected and transmitted SFG from the interfaces interested such as those reported recently by Richter et al. for the PS/SiO_2/Au system.[27,28] We will discuss only the SFG results for the samples with two typical PS thicknesses of 7 and 90 nm below according to the SFG results shown in Figure 4.

To determine exactly the origin of those SFG signals, these two polymer samples were exposed to an Ar-plasma treatment (PDC-3XG, Harrick, 30 W) and were then characterized by SFG measurements. Figure 5 shows the SFG spectra of (a) PMEA/PS7nm/Au and (b) PMEA/PS90nm/Au in the C−H stretching region for both PMEA and PS (2750−3100 cm^{-1}) by filled circles. Before the Ar-plasma treatment, the spectra were similar to those shown in Figure 4. After a 5 s Ar-plasma treatment, the SFG spectrum of PMEA/PS7nm/Au significantly changed whereas that of PMEA/PS90nm/Au was almost the same (Figure 5, open circles). An additional 5 s Ar-plasma resulted in similar SFG spectra. These results provide strong evidence that the SFG spectrum for PMEA/PS7nm/Au mainly comes from the air/PMEA interface while that of PMEA/PS90nm/Au mainly arises from the buried PMEA/PS interface (although we could not deny the possible contribution from free interface only by the above Ar-plasma treatment for the later case). It can be shown that the contribution from the PS/Au interface is negligible in comparison with that of the air/PMEA or PMEA/PS interface based on the local electric field calculation.[6] Although detailed experiments and calculation are still necessary to find the best contrast between the free and buried interfaces by optimizing the thickness of PS as well as that of PMEA,[29] we use the PMEA/PS7nm and PMEA/PS90nm/Au to probe the molecular structures on the free and buried PMEA interfaces, respectively, in the present work.

2.2. Orientation Changes in the OCH_3 at the PMEA Interfaces Induced by BPA Absorption. Figure 6 shows the SFG spectra (open circles) and fitted results (solid lines) for (i) PMEA/dPS7nm/Au and (ii) PMEA/dPS90nm/Au, respectively, in the regions for both C−H stretching and C−D stretching, (a) before and (b) after BPA absorption in a saturated (340 ppm) BPA

Table 3. Assignment and Deconvolution Results of SFG Spectra

			PMEA/dPS7nm/Au		PMEA/dPS90nm/Au	
ω_{IR}/cm^{-1}	assignment	Γ_n/cm^{-1}	before	after	before	after
2263	C−D ν_{20b}	6			0.06 ± 0.01	0.00 ± 0.02
2274	C−D ν_2	6			0.35 ± 0.02	0.12 ± 0.02
2822	OCH_3 ν_s	12	2.05 ± 0.07	3.06 ± 0.10	3.03 ± 0.09	1.34 ± 0.05
2842	CCH_2 ν_s	16	2.10 ± 0.09	2.84 ± 0.11	2.95 ± 0.11	1.39 ± 0.06
2880	CCH_3 ν_s	12		0.16 ± 0.07		0.00 ± 0.05
2899	OCH_2 ν_s	12	0.84 ± 0.05	1.57 ± 0.09	0.95 ± 0.07	0.58 ± 0.05
2924	CCH_2 ν_{as}	16	0.86 ± 0.07	1.19 ± 0.12	0.05 ± 0.09	0.21 ± 0.07
2940	CCH_3 $\nu_{s,FR}$	12		0.82 ± 0.12		0.07 ± 0.07
2957	OCH_2 ν_{as}	12	2.65 ± 0.06	3.35 ± 0.11	3.17 ± 0.08	1.40 ± 0.08
2968	CCH_3 ν_{as}	12		0.00 ± 0.07		0.00 ± 0.07
2990	OCH_3 ν_{as}	12	0.80 ± 0.04	0.45 ± 0.05	0.78 ± 0.05	0.20 ± 0.04
3071	C−H ν_2	12		0.54 ± 0.06		0.18 ± 0.05
	NR		0.35 ± 0.00	0.56 ± 0.00	0.58 ± 0.00	0.42 ± 0.00

[a] ω_{IR}: peak position. Γ_n: bandwidth. s: symmetric. as: asymmetric. FR: Fermi resonance. NR: nonresonance.

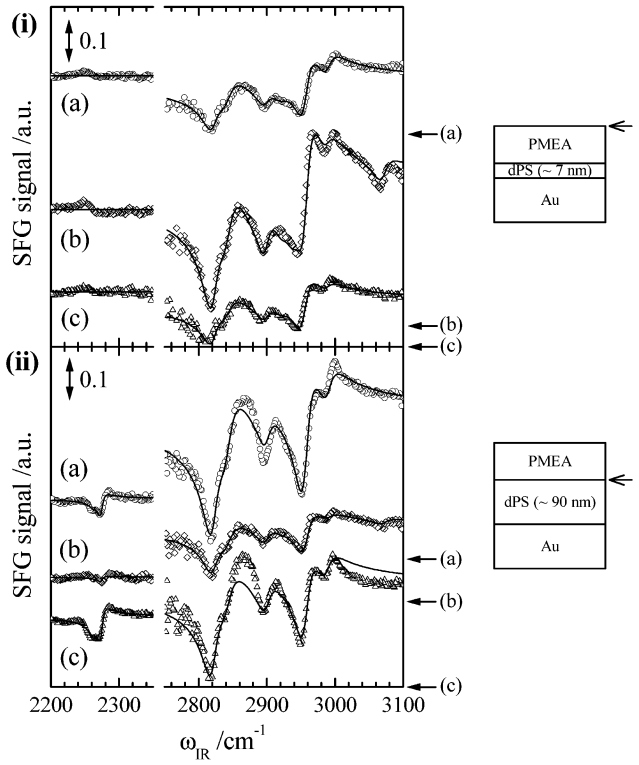

Figure 6. SFG spectra (symbols) and fitting results (solid lines) of PMEA/dPS7nm/Au (i) and PMEA/dPS90nm/Au (ii): (a) before dipping, (b) after 10 s dipping in a saturated BPA solution, and (c) after rinsing sample b with ethanol after dipping. The zero level of each spectra is shown by arrows on the right side.

aqueous solution for 10 s and (c) after rinsing with ethanol. The zero points for each curve were shifted vertically for clarity.

The deconvolution results are summarized in Table 3 together with the assignments.[14] The resonance and NR SFG signals from PMEA/dPS7nm/Au were weaker than those from PMEA/dPS90nm/Au. The SFG peaks at 2220 and 2274 cm^{-1} attributed to the phenyl ring C−D stretching ν_{20b} and ν_2 mode from dPS were clearly observed on PMEA/dPS90nm/Au (Figure 6ii(a)) but not on PMEA/dPS7nm/Au (Figure 6i(a)). On the basis of the thickness dependent SFG spectra discussed in Figures 4 and 5, this behavior can be understood by the SFG contribution being dominated by different interfaces; i.e., PMEA/ dPS7nm/Au is due to the free PMEA interface while PMEA/dPS90nm/Au is mainly due to the buried PMEA/PS interface.

When the PMEA was immersed into a saturated BPA solution, large changes were observed in the SFG spectra (Figure 6, parts i(b) and ii(b)). A new peak around 3071 cm^{-1}, which can be attributed to the aromatic ring C−H stretching ν_2 mode from BPA molecules, was observed on both PMEA/dPS7nm/Au and PMEA/dPS90nm/Au after the BPA immersion process, suggesting that an ordered adlayer of BPA was formed on both the free and buried PMEA interfaces.

After the surface was rinsed with ethanol (Figure 6, parts i(c) and ii(c)), the peaks due to BPA disappeared completely and the SFG spectra recovered to almost the same as those before BPA absorption, suggesting that the structural changes at both free and buried PMEA interfaces induced by BPA absorption are reversible, which agreed well with the IRRAS results shown in Figure 2.

In the following, the orientation angle and its distribution of the OCH_3 group for both free and buried interfaces will be deduced quantitatively from these SFG spectra.

Assuming an azimuthally isotropic interface, we have four independent nonvanishing components for the second nonlinear susceptibility, $\chi_{yyz} = \chi_{xxz}$, $\chi_{yzy} = \chi_{xzx}$, $\chi_{zyy} = \chi_{zxx}$ and χ_{zzz}.[6] The orientation angle (θ) of the OCH_3 group in the side chain of the PMEA is defined as the angle between the surface normal and the symmetric axis of the OCH_3 group. Considering the OCH_3 group with a C_{3v} symmetry, the second nonlinear susceptibility in a laboratory coordinate system (χ_{ijk}: χ_{xyz}) can be related to the molecular hyperpolarizability in the molecular coordinate system ($\beta_{\alpha\beta\gamma}$: β_{abc}) as follows. For the symmetric C−H stretching mode, we have[30,31]

$$\chi_{yyz,s} = \frac{1}{2}N_s\beta_{ccc}[\langle\cos\theta\rangle(1 + r) - \langle\cos^3\theta\rangle(1 - r)] \quad (2a)$$

$$\chi_{yzy,s} = \frac{1}{2}N_s\beta_{ccc}[\langle\cos\theta\rangle - \langle\cos^3\theta\rangle](1 - r) \quad (2b)$$

and for the asymmetric C−H stretching modes, we have

$$\chi_{yyz,as} = -\frac{1}{2}N_s\beta_{caa}[\langle\cos\theta\rangle - \langle\cos^3\theta\rangle] \quad (3a)$$

$$\chi_{yzy,as} = \frac{1}{2}N_s\beta_{caa}\langle\cos^3\theta\rangle \quad (3b)$$

where N_s is the surface density of the functional group and $r = \beta_{aac}/\beta_{ccc}$. It is difficult to consider that all the surface groups have the same orientation angle (i.e., δ-function distribution); therefore, the terms $F(\theta)$ in the

braces ⟨...⟩ in the above equation are employed for an ensemble average of the orientation angle by a distribution function $f(\theta)$:

$$\langle F(\theta)\rangle = \int_0^{\pi} F(\theta) f(\theta) \sin\theta \, d\theta \tag{4}$$

The Gaussian function is normally employed for the distribution function as

$$f(\theta) = C \exp\left[\frac{(\theta - \theta_0)^2}{2\sigma^2}\right] \tag{5}$$

where θ_0 is the mean orientation angle, C is a normalization constant, and σ is the root-mean-square width.

Because the intensities of SFG spectra with ssp- and sps-polarization can be directly related to χ_{yyz} and χ_{yzy}, respectively, the ratio (R) between $\chi_{yyz,as}$ and $\chi_{yzy,as}$ can be obtained from the C−H asymmetric stretching modes of the OCH_3 group observed from the two SFG spectra from eq 3, parts a and b, considering the correction on the local field, we have

$$R = \frac{\chi_{yyz,as}}{\chi_{yzy,as}} \times \frac{F_{ssp}}{F_{sps}} = -\frac{\langle\cos\theta\rangle - \langle\cos^3\theta\rangle}{\langle\cos^3\theta\rangle} \tag{6}$$

where F_{ssp} and F_{sps} are the Fresnel coefficients. By comparing the experimentally measured value R with the calculated results from eq 6, the orientation angle and its distribution for the OCH_3 can be deduced. In fact, many groups have undergone the estimation for the orientation angle of the surface methyl moiety by this method. Shen and his colleagues quantitatively estimated the orientation and its distribution in a rubbed poly(vinyl alcohol) (PVA) in this way and found that the PVA surface was fairly well ordered after rubbing.[23,32] Chen and co-workers deduced the ranges of the orientation angle and its distribution of the ester methyl group in the side chain of the PMMA[33] and PBMA surface.[26] They found that the orientation distribution of the ester methyl group on the PBMA surface becomes narrower in water than that in air.[26]

In the calculation by eq 6, two SFG spectra with ssp and sps-polarization are required. Unfortunately, we are still unable to obtain a reliable sps-polarized SFG spectrum in the present work. One of the possible reasons for this may be related to the weak s-polarized infrared electric field on the metal (Au) surface. Hence, we could not deduce the orientation angle and its distribution of the OCH_3 by eq 6 as those carried out by other groups in the present study. On the other hand, another analysis using the ratio ($R' = A_{ssp,as}/A_{ssp,s}$) can be obtained from eqs 2a and 3a where only the ssp-polarized SFG spectra are related

$$R' = \frac{\chi_{yyz,as}}{\chi_{yyz,s}} = \frac{\langle\cos\theta\rangle - \langle\cos^3\theta\rangle}{\langle\cos\theta\rangle(1+r) - \langle\cos^3\theta\rangle(1-r)} \times \frac{\beta_{caa}}{\beta_{ccc}} \tag{7}$$

Although R' is independent of the Fresnel coefficients, a number of unknown parameters (r, β_{caa}/β_{ccc}) are included in the equation. The ratio for β_{caa}/β_{ccc} was reported to be close to unity.[30] Dhinojwala et al. investigated the molecular structure of side chains of the comb polymer (poly(vinyl octadecyl carbamate-*co*-vinyl acetate)) at air interface[34] and reported that R' obtained from the SFG measurement is not sensitive to the r value of methyl group between 4.2 and 1.6

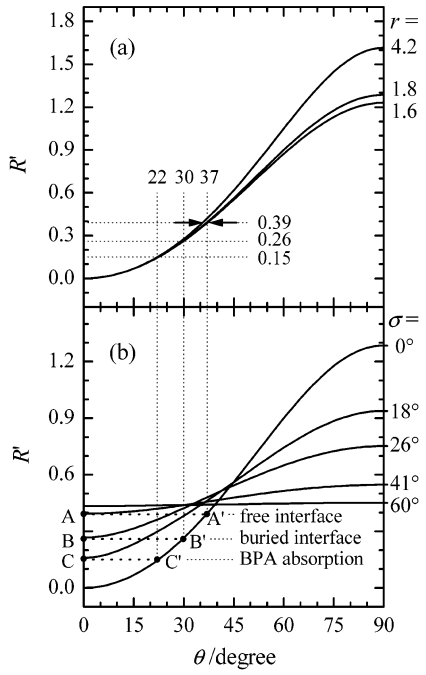

Figure 7. Calculation curves of eq 7: (a) with different ratios r of 1.6, 1.8, and 4.2 assuming $\sigma = 0$; (b) with different distributions σ of 0, 18, 26, 41 and 60° on θ assuming a Gaussian function and $r = 1.8$. $\sigma = 0$ corresponds to the δ-function.

Table 4. Observed Values of R' and Calculated Values of θ from Eq 7

	dipping in BPA	R'	θ/deg minimum	θ/deg maximum[a]
PMEA/dPS7nm/Au	before	0.39	0 ($\sigma \sim 41°$)	37
	after	0.15	0 ($\sigma \sim 18°$)	22
PMEA/dPS90nm/Au	before	0.26	0 ($\sigma \sim 26°$)	30
	after	0.15	0 ($\sigma \sim 18°$)	22

[a] Corresponds to the δ function ($\sigma \sim 0°$).

(assuming a δ-distribution) which is normally reported in references.[30,35−37] Recently, Chen et al. estimated the r value for the OCH_3 group in PMMA to be ca. 1.8 from SFG measurement.[33]

Figure 7(a) shows the calculated R' ($A_{ssp,as}/A_{ssp,s}$) estimated by eq 7 assuming a δ-function angle distribution ($\sigma = 0°$) for a different value of r (1.6−4.2). Values of R' for the OCH_3 group in PMEA/dPS7nm/Au (Figure 6i(a)) and PMEA/dPS90nm/Au (Figure 6ii(a)) were determined to be 0.39 and 0.25, respectively (Table 4). Fortunately, as clearly shown in Figure 7a, the r dependence is not as remarkable for the observed R' region ($R' < 0.39$). Similar comparisons were also carried out for the angle distribution with the Gaussian function with $\sigma < 60°$, and the r dependence became slightly larger but may be sufficient for the purpose in the present work. In the following quantitative analysis on the orientation angle of the OCH_3 group in PMEA before and after BPA absorption, we assume $r = 1.8$.

Figure 7b shows the calculated R' by eq 7 as a function of θ with the Gaussian angle distribution ($\sigma = 0-60°$). The experimentally observed results for R' (Table 4) are also shown in the same figure by the dotted lines. On the free PMEA interface ($R' = 0.39$), the orientation angle and its distribution should fall between point A and A' (Figure 7b), i.e., θ_0 of 0° with an angle distribution of $\sigma = 41°$ (A) and θ_0 of 37° with a

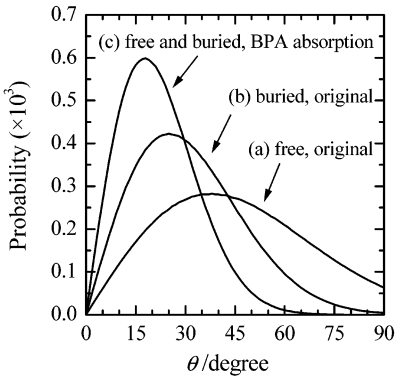

Figure 8. Orientation probability density function with different σ values of (a) 41° (point *A* in Figure 7b), 26° (point *B*), and 18° (point *C*) at $\theta_0 = 0°$.

δ-angle distribution (*A*′). At the buried PMEA interface ($R' = 0.25$), the orientation angle should fall in the region *BB*′ (Figure 7b), i.e., $\theta_0 = 0°$ with $\sigma = 26°$ (*B*) and $\theta_0 = 30°$ with $\sigma = 0°$ (*B*′). On the average, the orientation of the OCH_3 group at the buried PMEA/PS interface seems to be more perpendicular to the surface, and its ordering is likely higher than that on the free PMEA interface due to the smaller angle distribution.

As shown in Figure 6 and Table 4, the values of *R*′ decreased to 0.15 after immersion in BPA solution at both the free and buried interfaces. Therefore, the orientation angle and its distribution should fall in the region *CC*′ (Figure 7b) of $\theta_0 = 0°$ with $\sigma = 18°$ (*C*) and $\theta_0 = 22°$ with $\sigma = 0°$ (*C*′). The mean orientation angle θ_0 and the angle distribution becomes smaller in comparison with those before BPA absorption. Figure 8 shows the orientation distribution population of the OCH_3 group with the maximum angle distribution (σ) (i.e., minimum mean orientation angles θ_0) at the free and buried PMEA interfaces before and after BPA absorption (i.e., corresponding to points *A*, *B*, *C* in Figure 7b). Although we are unable to determine an absolute orientation angle for the OCH_3 group at the PMEA interface, it is straightforward from this figure that the angle distribution of the OCH_3 group at both the free and buried PMEA interfaces becomes much smaller after BPA absorption. The present results indicate that the OCH_3 group becomes more ordered and should stand up on both interfaces after BPA absorption. It is expected that the polymer packing density increases and that the mobility of the side chain of the PMEA decreases by the hydrogen-bonding interaction between BPA molecules and the PMEA thin film. Consequently, the orientation of the OCH_3 group at the PMEA interfaces becomes more perpendicular to the surface with a narrower angle distribution.

After the polymer surface was rinsed with ethanol (Figure 6, parts i(c) and ii(c)), the peaks due to BPA disappeared completely, and the SFG spectrum recovered to its original shape (i.e., before absorption). Values of *R*′ were the same as those before BPA absorption, suggesting that the structural changes at both the free and buried PMEA interfaces induced by BPA absorption are reversible.

On the other hand, although the orientation angle and its distribution have been estimated above, we need to consider the relative orientation direction of the OCH_3 group of PMEA and the phenyl ring of PS at both the free and buried PMEA interfaces. Richter et al. reported that the pendant phenyl groups of PS at the free PS/air and buried PS/SiO_2 interfaces are pointed away from the bulk PS, i.e., the phenyl group at the free interface points into the air while that at the buried interface points into SiO_2.[24,27,28] Chen et al. reported that the ester side chain methyl groups tend to stand up on the PBMA surface in air, but at the PBMA/PS interface, the ester side chain methyl tend to lie down on the surface.[26] The preliminary calculations for our PMEA/PS/Au system show that the relative phase of the Fresnel coefficients at the free and buried PMEA interfaces are same (0) for a PS thickness between 0 and 150 nm. Because the free PMEA interface also partly contributes to the SFG spectra at thicknesses between 56 and 153 nm (Figure 4c−f), it is expected that the orientation vector of the OCH_3 group in PMEA at the two interfaces is in the same direction with respect to the Au. Otherwise, the intensity of the SFG peak should decrease due to the reversed dipole direction. The opposite SFG peak position for PS at PS thickness of 220 nm can be attributed to the relative phase change (π) of the Fresnel coefficients at the buried PMEA/PS interface around this thickness.[29] On the other hand, the appearance of both ν_{20b} and ν_2 modes demonstrated that the phenyl groups of PS (Figures 5b and 6ii(a)) should tend to lie down and is similar to that observed at the PBMA/PS interface[26] but different from that at the PS/air interface.[24,25] After immersion in BPA solution, only the ν_2 mode can be observed (Figure 6ii(b) and Table 3), suggesting that the phenyl groups of PS tend to stand up. The phenyl groups of PS on the PMEA/PS interface tend to lie down again after BPA desorption.

Finally, one should note that the resonance and the NR SFG signals for PMEA/dPS7nm/Au increased while those for PMEA/dPS90nm/Au decreased after the BPA immersion process (Figure 6 and Table 4). The ellipsometry measurements show that PMEA swells by ca. 35 nm in thickness on the PMEA/dPS7nm/Au after immersion in a saturated BPA aqueous solution for 10 s (Figure 3). In comparison with the results shown in Figure 4, these changes in the intensities of the SFG signals can be attributed to thickness changes in the PMEA film as a result of the swelling process induced by BPA absorption: SFG resonance and NR signals are roughly expected to increase for PMEA/dPS7nm/Au but decrease for PMEA/dPS90nm/Au while the peak contributions are almost the same after this swelling process.

2.3. Reasons for the Selective Absorption of BPA in PMEA Thin Film. It is essential to determine the reasons for the different penetration and adsorption behavior of BPA molecules in PMEA, PMMA, and PS thin films. As observed by the IRRAS spectra, hydrogen bonding is formed between the hydroxyl group in BPA molecules and the carbonyl group in PMEA (Figure 2b). Hydrogen bonding is one of the important factors keeping BPA stable in the PMEA thin film. Similar hydrogen bonding was also found in the mixed film of PMMA and BPA (spectrum is not shown here); however, BPA absorption was not observed in the PMMA film. Therefore, other factors should play roles in the BPA absorption process. In fact, PMEA shows a much lower glass transition temperature (T_g), ∼−50 °C,[38] in comparison with that of PMMA (∼105 °C) and PS (∼100 °C).[39] The penetration of BPA into the polymer bulk can be affected by the micro-Brownian motion of polymer main-chain and its free volume, which are related to T_g. The structure of a polymer with a higher T_g will be

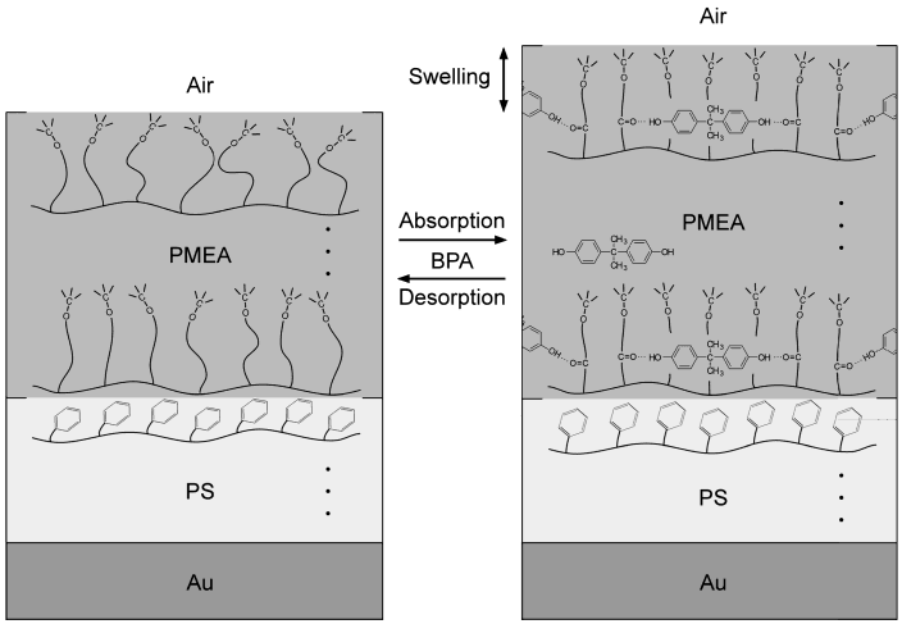

Figure 9. Schematic model for orientation changes at the polymer interface induced by BPA adsorption and desorption.

more rigid and other molecules will not easily penetrate. The lower the T_g, the higher is the mobility of absorbed molecules in the polymer bulk, the easier is the structure change and, therefore, the higher is the absorbed amount. Chen et al. also reported that the surface structure of poly(methacrylate)s in water strongly depends on its relative value of T_g.[40]

On the other hand, a small peak at 3071 cm^{-1} was newly observed at the PMMA/air interface after BPA immersion (the SFG spectrum is not shown here), which can be attributed to BPA adsorbed on the PMMA surface as was observed at the PMEA surface (Figure 6i(a)). No change was observed at the dPS surface after the immersion, suggesting that BPA does not adsorb on the dPS surface. Therefore, although BPA molecules cannot penetrate into the bulk of PMMA and PS due their higher T_g, BPA can adsorb on the surface of PMMA due to hydrogen bonding between BPA and PMMA. However, BPA adsorption was not found on the PS surface, and this may be related to the much weaker interaction between PS and BPA than that between PMMA and BPA. As we will mention elsewhere the hydrophobic property of the BPA molecule also plays a role in the selective absorption in PMEA thin film.[18] The interaction between the BPA and PMEA is not very strong, and the absorbed BPA molecules could be removed from the polymer with ethanol.

Conclusions

The molecular structure changes in PMEA thin films induced by the absorption of BPA have been investigated by IRRAS and SFG measurements in comparison with PMMA and PS thin films. BPA molecules were absorbed in PMEA but not in PMMA and PS thin films, and absorbed BPA can be removed from the PMEA by an ethanol rinsing treatment. Hydrogen bonding was formed between the hydroxyl group of BPA and carboxyl group of the PMEA.

By controlling the thickness of a PS layer sandwiched between PMEA and the Au substrate, we are able to selectively measure the molecular structures at the different polymer interfaces at air/PMEA and the buried PMEA/PS substrate. Figure 9 shows a schematic model illustrating the above features. The OCH_3 group in the side chain of PMEA at both interfaces has the opposite vector orientation with respect to the bulk of PMEA, i.e., pointing into air at the free interface and pointing into PMEA at the PMEA/PS buried interface. The orientation distribution of the OCH_3 group at the buried interface is smaller than that at the free interface, suggesting a higher ordering at the PMEA/PS interface. When BPA was absorbed into the PMEA, the orientation of the OCH_3 group in PMEA on both interfaces became more perpendicular to the surface and its distribution also becomes narrower, indicating that the interfacial ordering increased; the phenyl groups of PS tend to stand up on the buried PMEA/PS interface. The BPA absorption-induced orientation changes are reversible.

The different absorption behavior of BPA in PMEA, PMMA and PS thin films can be related to their differences in T_g. The lower the T_g, the easier is the BPA penetration into the polymer. The hydrogen bonding between the BPA and poly(acrylate)s also contributes to the affinity of BPA for PMEA and PMMA.

Acknowledgment. S.Y. greatly acknowledges the support from PRESTO, Japan Science and Technology Corporation (JST). S.Y. also wants to acknowledge the support from the SHISEIDO Fund for Science and Technology and 2001 Corning Research Grants. We thank Prof. Shimazu for help with the Ar-plasma treatment. We want to think Dr. Richter for his help in the calculation of the Fresnel coefficients in the multilayer system.

References and Notes

(1) Wright, A. N.; Fischli, A. E. *Pure Appl. Chem.* **1998**, *70*, 1617−1865.
(2) Hunt, P. A.; Koehler, K. E.; Susiarjo, M.; Hodges, C. A.; Ilagan, A.; Voigt, R. C.; Thomas, S.; Thomas, B. F.; Hassold, T. J. *Curr. Biol.* **2003**, *13*.
(3) Tanaka, M.; Motomura, T.; Kawada, M.; Anzai, T.; Kasori, Y.; Shiroya, T.; Shimura, K.; Onishi, M.; Mochizuki, A. *Biomaterials* **2000**, *21*, 1471−1481.
(4) Mueller, X. M.; Jegger, D.; Augstburger, M.; Horisberger, J.; von Segesser, L. K. *Int. J. Artif. Organs* **2002**, *25*, 223−229.

(5) Suetaka, W. *Surface infrared and Raman spectroscopy, methods and applications*; Plenum Press: New York, 1995.
(6) Shen, Y. R. *The Principles of Nonlinear Optics*; John Wiley & Sons: New York, 1984.
(7) Buck, M.; Himmelhaus, M. *J. Vac. Sci. Technol. A* **2001**, *19*, 2717−2736.
(8) Richmond, G. L. *Chem. Rev.* **2002**, *102*, 2693−2724.
(9) Chen, Z.; Shen, Y. R.; Somorjai, G. A. *Annu. Rev. Phys. Chem.* **2002**, *53*, 437−465.
(10) Ye, S.; Noda, H.; Morita, S.; Uosaki, K.; Osawa, M. *Langmuir* **2003**, *19*, 2238−2242.
(11) Ye, S.; Nihonyanagi, S.; Uosaki, K. *Phys. Chem. Chem. Phys. (PCCP)* **2001**, *3*, 3463−3469.
(12) Azzam, R. M. A.; Bashara, N. M. *Ellipsometry and Polarized Light*; North-Holland: Amsterdam, 1977.
(13) Uosaki, K.; Kondo, T.; Okamura, M.; Song, W. *Faraday Discuss.* **2002**, *121*, 373−389.
(14) Colthup, N. B.; Daly, L. H.; Wiberley, S. E. *Introduction to Infrared and Raman Spectroscopy*, 3rd ed.; Academic Press Inc.: San Diego, CA, 1990.
(15) Lipschitz, I. *Polym. Plast. Technol. Eng.* **1982**, *19*, 53−106.
(16) Dybal, J.; Krimm, S. *Macromolecules* **1990**, *23*, 1301−1308.
(17) Wilson, E. B. *Phys. Rev.* **1934**, *45*, 706−714.
(18) Li, G. F.; Morita, S.; Ye, S.; Tanaka, M.; Osawa, M. Submitted for publication.
(19) Dong, J.; Ozaki, Y. *Macromolecules* **1997**, *30*, 286−292.
(20) Du, Q.; Superfine, R.; Freysz, E.; Shen, Y. R. *Phys. Rev. Lett.* **1993**, *70*, 2313−2316.
(21) Du, Q.; Freysz, E.; Shen, Y. R. *Science* **1994**, *264*, 826−828.
(22) Miranda, P. B.; Shen, Y. R. *J. Phys. Chem. B* **1999**, *103*, 3292−3307.
(23) Wei, X.; Zhuang, X.; Hong, S. C.; Goto, T.; Shen, Y. R. *Phys. Rev. Lett.* **1999**, *82*, 4256−4259.
(24) Briggman, K. A.; Stephenson, J. C.; Wallace, W. E.; Richter, L. J. *J. Phys. Chem. B* **2001**, *105*, 2785−2791.
(25) Gautam, K. S.; Schwab, A. D.; Dhinojwala, A.; Zhang, D.; Dougal, S. M.; Yeganeh, M. S. *Phys. Rev. Lett.* **2000**, *85*, 3854−3857.
(26) Chen, C. Y.; Wang, J.; Even, M. A.; Chen, Z. *Macromolecules* **2002**, *35*, 8093−8097.
(27) Wilson, P. T.; Briggman, K. A.; Wallace, W. E.; Stephenson, J. C.; Richter, L. J. *Appl. Phys. Lett.* **2002**, *80*, 3084−3086.
(28) Wilson, P. T.; Richter, L. J.; Briggman, K. A.; Stephenson, J. C. *Chem. Phys. Lett.* **2002**, *363*, 161−168.
(29) Ye, S.; Morita, S.; Li, G.; Osawa, M. To be submitted for publication.
(30) Watanabe, N.; Yamamoto, H.; Wada, A.; Domen, K.; Hirose, C. *Spectrochim. Acta* **1994**, *50A*, 1529−1537.
(31) Hirose, C.; Akamatsu, N.; Domen, K. *Appl. Spectrosc.* **1992**, *46*, 1051−1072.
(32) Wei, X.; Hong, S. C.; Zhuang, X.; Goto, T.; Shen, Y. R. *Phys. Rev. E* **2000**, *62*, 5160−5172.
(33) Wang, J.; Chen, C.; Buck, S.; Chen, Z. *J. Phys. Chem. B* **2001**, *105*, 12118−12125.
(34) Gautam, K. S.; Dhinojwala, A. *Macromolecules* **2001**, *34*, 1137−1139.
(35) Zhang, D.; Gutow, J.; Eisenthal, K. B. *J. Phys. Chem.* **1994**, *98*, 13729−13734.
(36) Wolfrum, K.; Laubereau, A. *Chem. Phys. Lett.* **1994**, *228*, 83−88.
(37) Zhuang, X.; Miranda, P. B.; Kim, D.; Shen, Y. R. *Phys. Rev. B* **1999**, *59*, 12632−12640.
(38) Tanaka, M.; Motomura, T.; Ishii, N.; Shimura, K.; Onishi, M.; Mochizuki, A.; Hatakeyama, T. *Polym. Int.* **2000**, *49*, 1−5.
(39) Brandrup, J.; Immergut, E. H.; Grulke, E. A. *Polymer Handbook*; Wiley: New York, 1999.
(40) Wang, J.; Woodcock, S.; Buck, S.; Chen, C.; Chen, Z. *J. Am. Chem. Soc.* **2001**, *123*, 9470−9471.

MA026007D